Indian Journal of Pure & Applied Physics
Vol. 62, March 2024, pp. 222-228
DOI: 10.56042/ijpap.v62i3.6654

Effect of Pressure and Squeezed-film Damping on Transient Response of a Double-Bridge Micromirror for Multiobject Spectroscopy

Amit Kumar[a,b]*, Deepak Bansal[a,b] & Kamaljit Rangra[c]

[a]CSIR-Central Electronics Engineering Research Institute, Pilani, Rajasthan 333 031, India
[b]Academy of Scientific and Innovative Research (AcSIR), Ghaziabad 201 002, India
[c]Indian Institute of Technology Jodhpur, Rajasthan 342 037, India

Received 8 November 2023; accepted 1 January 2024

This paper presents an analytical approach to envisage a suitable operating pressure and investigate the effect of squeezed-film damping on the transient response of a micromirror of size 200 µm × 200 µm and a deflection of 2.5 µm for space-based multiobject spectroscopy. While most MEMS devices are vacuum packaged to achieve a high Q and fast switching, the same may not be true for applications that are prone to vibrations and shocks. At small pressures, the micromirror can produce undesired deflections and oscillations, and hence, a high-pressure operation becomes necessary to alleviate these effects.The operating pressure and its effect on the transient response of the micromirror are investigated by solving linearized Reynold's equation and dynamic equation of motion using the numerical iteration method. The result shows an overdamped response above 10 kPa pressure. At 101 kPa, the micromirror exhibits a switching and release time of 102 µs and 95 µs, respectively. The analytical results are very close to the FEM results with a deviation of 8%. The result shows that operating a micromirror at atmospheric pressure serves the dual purpose of dispensing away with the requirement of vacuum packaging and providing immunity from vibrations and oscillation.

Keywords: Micromirror; Squeezed-film damping; Quality factor; Switching time; Release time

Introduction

Microelectromechanical System (MEMS) electrostatically actuated micromirrors have found application in multiobject spectroscopy due to their small size, low power consumption, and dynamic reconfiguration capability[1,2]. The latest trend is towards small driving voltages to facilitate integration with the onboard voltage supply. A micromirror with a large aperture, high fill factor, and small actuation voltage is essential in multiobject spectroscopy to deflect the incoming light from distant space targets toward the spectrograph[3]. The authors have demonstrated a large aperture, electrostatically-actuated double-bridge micromirror with hidden cantilever architecture for the multiobject spectroscopy[4]. The double-bridge design is referred herein to the two overlying structural layers *i.e.* supporting cantilevers and the top mirror plate suspended over the actuation electrodes[5] as shown in Fig. 1. An analytical model is developed to optimize the pull-in voltage below 25 V for an aperture size of 200 µm × 200 µm and an actuation gap of 2.5 µm to make it integration-compatible with the standard 28 V DC supply bus available for the electronic systems in the spacecraft[6]. The double-bridge micromirror fabricated using surface micromachining exhibits a bigger aperture and more degrees of freedom (2-axis rotation and piston motion) than the conventional 1-axis, double-bridge micromirrors available in the literature for multiobject spectroscopy[5].

The authors demonstrated the effect of different parameters on the static behavior[4]; however, the transient behavior of the micromirror was not investigated. Vacuum packaging is traditionally used for different MEMS devices to achieve a high-quality factor and fast switching speeds depending on the application requirements; however, the same may not be true forspace-based applications, prone to vibrations and shocks[7]. A low-pressure operation of micromirror in the space-based application would result in unwanted deflection due to random vibrations and sustained oscillations after state transitions. Operating the micromirror above a threshold pressure can offer a viable approach to prevent unwanted movements by compromising the quality factor. Since the energy dissipation from

*Corresponding author: (E-mail: amitkumar@ceeri.res.in)

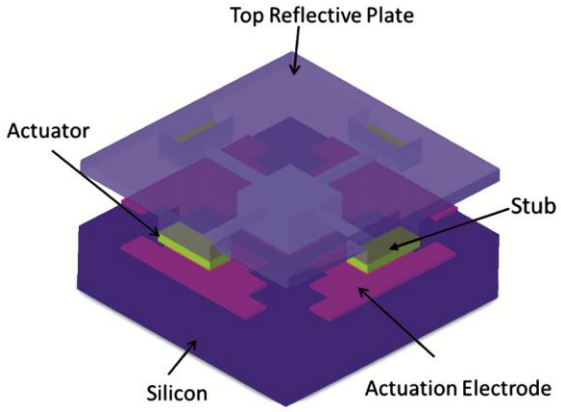

Fig. 1 — Double-bridge micromirror design[5].

pressure-induced squeezed-film damping also affects the transient behavior, accurately predicting its effects on the switching and release time of the micromirror becomes necessary. Authors have modeled the squeezed-film damping using a Green's function approach to investigate the spring constant of complex geometries at different venting conditions without performing any transient analysis[8]. The effect of pressure-induced squeezed-film damping on the resonant behavior of pressure sensors was investigated; however, no transient analysis was done[9,10]. The dynamic motion of a torsional micromirror under squeezed-film damping effects was analyzed using a complex and mathematically intensive Fourier and double sine series method[11].

This paper presents an analytical approach to envisage a suitable operating pressure and investigate the effect of squeezed-film damping on the transient behavior of the double-bridge micromirror for reliable space-based multiobject spectroscopyapplications. To mitigate the effect of thermal residual stress, the supporting cantilevers and the mirror plate are designed using a single structural material *i.e.*, gold[5].The electrostatic force responsible for micromirror actuation is modeled using a parallel-plate approximation, and the squeezed-film damping effects are analyzed by solving the linearized Reynolds equation. The effect of operating pressure on switching and release time is investigated by solving the dynamic equation of motion using the Runga-Kutta numerical iteration method in Matlab®. The results show that operating the optimized micromirror design formultiobject spectroscopy application[4,5] above a threshold pressure *i.e.*, 10 kPa in the present case serves the dual purpose of dispensing away with the requirement of vacuum packaging and providing immunity from space vibrations and oscillation without adversely affecting the switching speeds. The analytically obtained switching and release time of 102 μs and 95 μs are compared with the FEM simulation results[4] and agree within 8%. The simple analytical approach presented in this paper can be used to optimize the operating pressure and analyze the effect of squeezed-film damping on the transient response of different MEMS structures.

1 Pull-in Voltage of Micromirror

The cross-section of the micromirror is shown in Fig. 2(a). The structure consists of flexible supporting cantilevers suspended ata height-*h* above the actuation electrodes. The reflective mirror plate is attached to the free ends of the cantilevers and a stub height-*g* provides an offset between the two during actuation. The cantilevers undergo bending upon applying a voltage between the actuation electrode and the suspended structure resulting in the deflection of the rigid mirror plate as shown in Fig. 2(b).

Following assumptions are made for the calculation of the pull-in voltage of the micromirror.

(i) The mirror plate is rigid and remains free from bending or deformation during actuation

(ii) The cantilevers are perfectly elastic and undergo small deflection

(iii) The effect of twisting cantilevers on the micromirror deflection is negligible compared to the bending cantilevers.

(iv) The two bending cantilevers have equal and symmetric deflection behavior, and the rotational axis remains fixed and passes through the center of the mirror plate.The total force on the micromirror consists of the forces between the mirror plate, cantilevers, and actuation electrode. The net force acting on the micromirror at equilibrium is given by Eq. 1.

$$\frac{1}{2}\frac{\varepsilon_o A_1 V^2}{(h-y)^2}+\frac{1}{2}\frac{\varepsilon_o A_2 V^2}{(h+g+t-y)^2}-ky=0 \qquad \ldots(1)$$

Where y is the deflection of the micromirror tip from its rest position, k is the spring constant, and $A_1$and A_2 are the overlap area of the cantilever and mirror plate with the actuation electrode. The actuation voltage of the micromirror is obtained by rearranging Eq. 1 and given by

$$V=\sqrt{\frac{ky}{\frac{1}{2}\frac{\varepsilon_o A_1}{(h-y)^2}+\frac{1}{2}\frac{\varepsilon_o A_2}{(h+g+t-y)^2}}} \qquad \ldots(2)$$

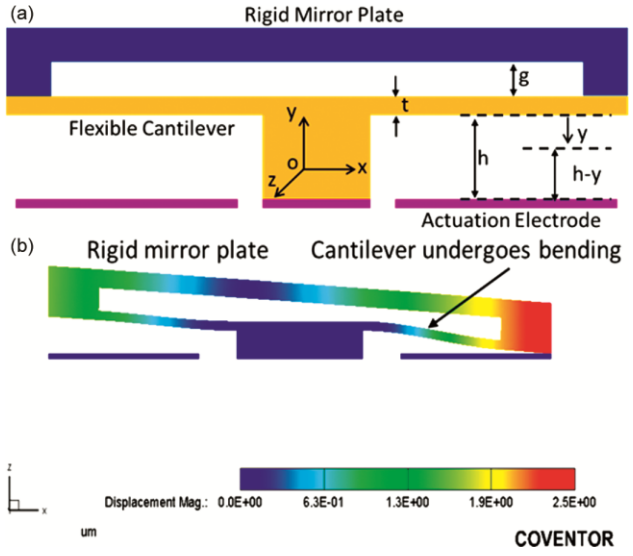

Fig. 2 — (a) Cross-sectional view of the double-bridge micromirror and (b) Bending of cantilevers and micromirror deflection.

The snap-down point of the micromirror at which the micromirror goes into a tilted state is obtained by differentiating Eq. 2 w.r.t.*y* and equating to zero, which gives

$$\frac{k\varepsilon_o A_1}{2(h-y)^2}\left(1-\frac{2y}{h-y}\right)+\frac{k\varepsilon_o A_2}{2(h+g+t-y)^2}\left(1-\frac{2y}{h+g+t-y}\right)=0 \quad \ldots (3)$$

Since the cantilever and mirror plate are at the same potential, the electrostatic field is mostly confined in the actuation gap-*h*. The contribution of the second term of Eq. 3 can be ignored, and the modified expression is given by Eq. 4.

$$\frac{k\varepsilon_o A_1}{2(h-y)^2}\left(1-\frac{2y}{h-y}\right)=0 \quad \ldots(4)$$

The snap-down point is obtained by solving Eq. 4 and substituting in Eq. 2 to get the pull-in voltage of the micromirror and given by

$$V_{Pull-in}=\sqrt{\frac{\frac{2}{3}\frac{Ehwt^3}{L^3}}{\frac{9}{8}\frac{\varepsilon_o A_1}{h^2}+\frac{9}{2}\frac{\varepsilon_o A_2}{(3g+3t-2h)^2}}} \quad \ldots(5)$$

Where *E* is Young's modulus, and *w*, *t*, and *L* are the cantilevers' width, thickness, and length. A mirror plate of aperture size 200 μm × 200 μm is considered for analysis as per the requirements of multiobject spectroscopy application[12]; however, the same approach is applicable for any aperture size. The

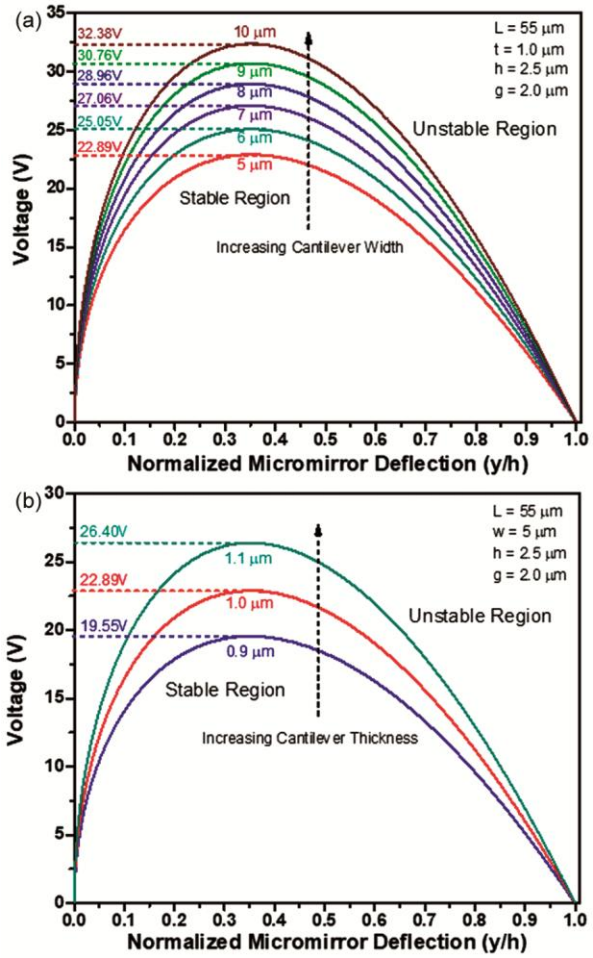

Fig. 3 — (a) Normalized deflection of micromirror (y/h) vs. voltage for different cantilever widths and (b) Different cantilever thicknesses.

cantilever length is fixed at 55 μm to ensure the hiding of cantilevers and anchor posts below the mirror plate to achieve a high fill factor. For all calculations, the actuation gap, and stub height are fixed at 2.5 μm, and 2.0 μm, respectively; however, it is also applicable for larger gaps till the cantilever deflections are with in the elastic limit and can be approximated by square-law curvature[13].

The micromirror deflection with voltage for different cantilever widths and thicknesses is shown in Fig. 3(a&b), respectively, where peaks of curves correspond to the pull-in voltage of the micromirror. The peak exhibits an upward shift with increasing cantilever widths and thicknesses due to increased cantilever stiffness. The calculation of the pull-in voltage is required to select a suitable actuation voltage for micromirror switching[14]. The cantilever design is optimized at 55 μm × 5 μm × 1 μm and an

equivalent spring constant of 4.81 N/m for a pull-in voltage of 22.89 V to ensure device integration with 28 V supply bus available in the spacecraft[6].

2 Squeezed-Film Damping and Pressure Optimization

The dynamic motion of the micromirror is given by Eq. 6

$$m\frac{d^2y}{dt^2}+b\frac{dy}{dt}+ky=\frac{1}{2}\frac{\varepsilon_o A_1 V^2}{(h-y)^2}+\frac{1}{2}\frac{\varepsilon_o A_2 V^2}{(h+g+t-y)^2} \quad \ldots(6)$$

Where m is the mass of the suspended structure, and b is the damping coefficient. Without damping, the micromirror may suffer from unwanted deflection due to random vibrations in the space-based environment. Also, the micromirror may suffer from multiple oscillations before coming to a steady state leading to unreliable operation. Operating the micromirror above a threshold pressure results in damping by squeezed-in and out movement of air below the mirror plate[15] as shown in Fig. 4. A resistive force is generated that opposes the mirror movement and prevents unwanted deflection and oscillations[16]. The squeezed-film damping effect is governed by the Reynolds equation[17].

At isothermal conditions, the air density-ρ is proportional to the pressure-P, and the modified Reynolds equation is given by Eq. 7.

$$\frac{\partial}{\partial x}\left(P\frac{\partial P}{\partial x}\right)+\frac{\partial}{\partial y}\left(P\frac{\partial P}{\partial y}\right)=\frac{12\mu}{h^3}\frac{\partial(hP)}{\partial t} \quad \ldots(7)$$

The pressure effect is analyzed by solving the linearized Reynolds equation, and the rarefaction effect is accounted for by substituting the dynamic viscosity-μ with effective viscosity-μ_e in Eq. 7. Various expressions for μ_e have been proposed by different authors[18–20]; however, the expression proposed by Veijola[21] is considered the most accurate over a wide range of Knudsen number-K_n. The squeeze parameters, i.e., cut-off frequency-f_c and squeeze number-σ are calculated to determine the compressibility of air trapped below the mirror plate[22]. The micromirror has a resonant frequency of 32.79 kHz[5], much smaller than the f_c for all pressure values, as shown in Fig. 5(a). The value of σ is also much smaller than the cut-off squeeze number of a square plate (σ_c=19.7), as shown in Fig. 5(b). The results show that air trapped below the mirror plate can be approximated as incompressible[22] for a wide range of operating pressures.

The quality factor is an important parameter that determines the amount of energy dissipated per cycle and is significantly affected by air damping. The quality factor of the micromirror at different pressures under incompressible fluid approximation is shown in Fig. 6(a). The threshold pressure above which the micromirror exhibits an overdamped response is

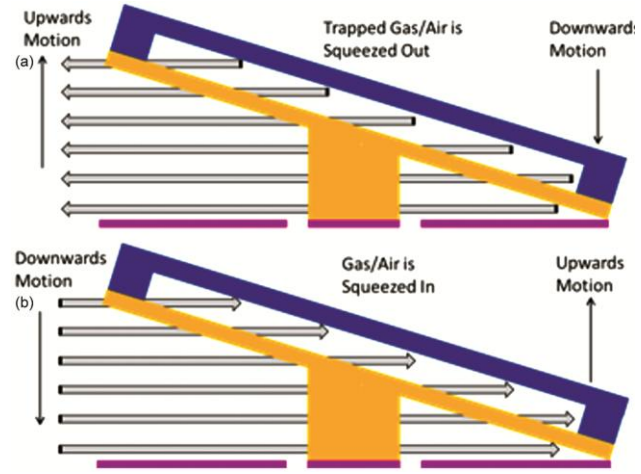

Fig. 4 — Squeezed-in and out movement of air.

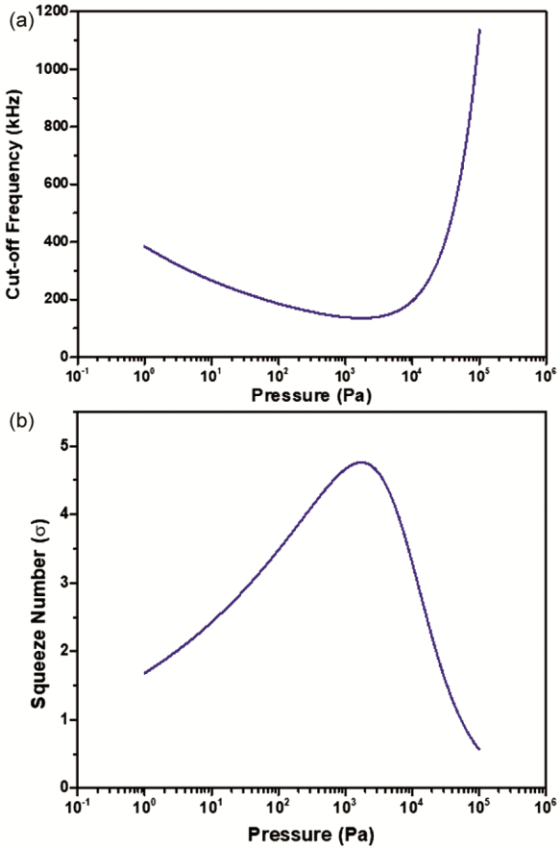

Fig. 5 — (a) Cut-off frequency of micromirror and (b) Squeeze number with pressure.

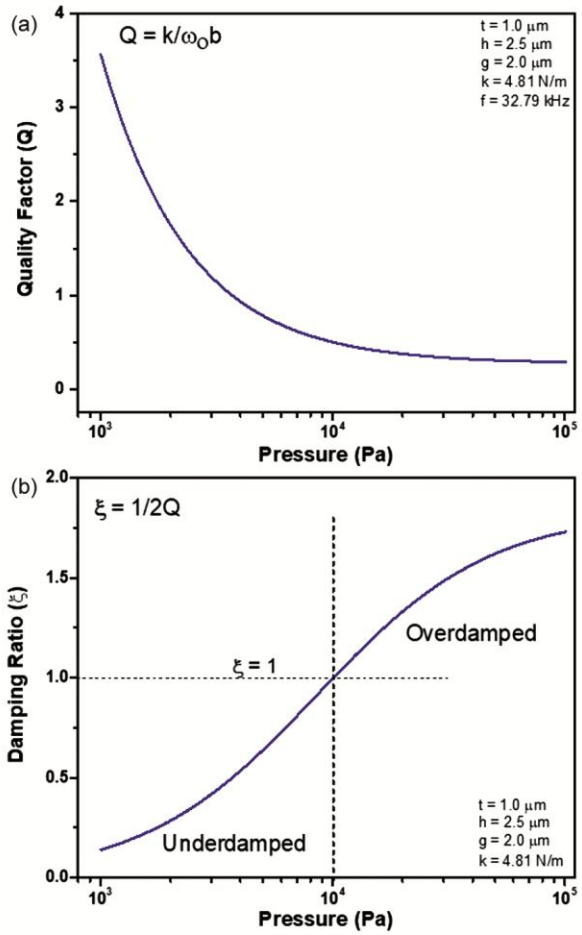

Fig. 6 — (a) Quality factor and (b) Damping ratio at different pressure.

calculated by locating the intersection of the ξ=1 line with the damping ratio curve as shown in Fig. 6(b).

The micromirror exhibits an overdamped behavior above 10 kPa pressure. The Runga-Kutta numerical iteration is further used to analyze the transient behavior of the micromirror by solving the dynamic equation of motion at different pressures. A correct prediction of the switching and release time of the micromirror at the operating pressure would ensure integration with the onboard voltage supply and driver circuit[23].

3 Switching and Release Time of Micromirror

The electrostatic force responsible for micromirror actuation is affected by the supply voltage, and it is a general practice to operate them at a voltage slightly higher than its pull-in voltage[14]. For the calculation of switching time, the second-order differential equation in Eq. 6is reduced to two first-order differential equations.

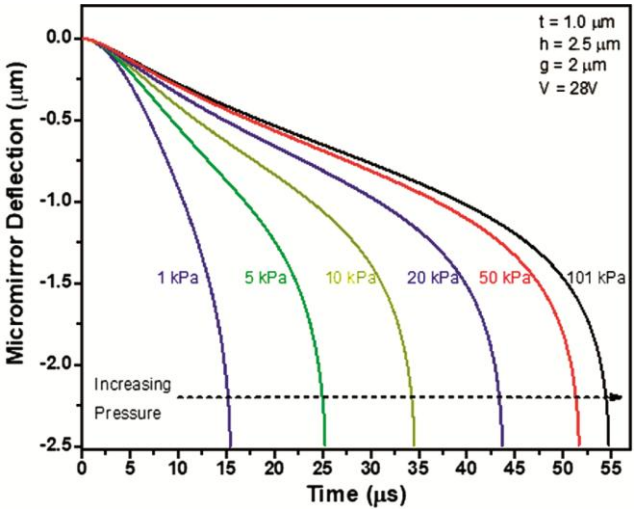

Fig. 7 — Micromirror deflection for different pressure.

$$\frac{dy}{dt} = x \qquad \ldots(8)$$

$$\frac{dx}{dt} = -\left(\frac{b}{m}\right)x - \left(\frac{k}{m}\right)y + \frac{1}{2}\left(\frac{\varepsilon_o A_1 V^2}{m(h-y)^2} + \frac{\varepsilon_o A_2 V^2}{m(h+g+t-y)^2}\right) \qquad \ldots(9)$$

The coefficients *b/m* and *k/m* in Eq. 9 are calculated at different pressures and applied as input parameters with the initial conditions of zero displacement and zero velocity given by

$$y(0) = 0 \qquad \ldots(10)$$

$$x(0) = 0 \qquad \ldots(11)$$

The switching response of the micromirror at different pressures is shown in Fig. 7. At 28 V, the micromirror exhibits a switching time of 34 μs at 10 kPa pressure. The switching time increases to 66 μs as the operating pressure is increased to 101 kPa pressure.

The effect of supply voltage on the switching time at different pressures is shown in Fig. 8. The results show a faster switching with increasing voltage and decreasing pressure.

The release time of the micromirror is obtained by removing the electrostatic force term in Eq. 6. The set of reduced first-order differential equations is given by

$$\frac{dy}{dt} = x \qquad \ldots(13)$$

$$\frac{dx}{dt} = -\left(\frac{b}{m}\right)x - \left(\frac{k}{m}\right)y \qquad \ldots(14)$$

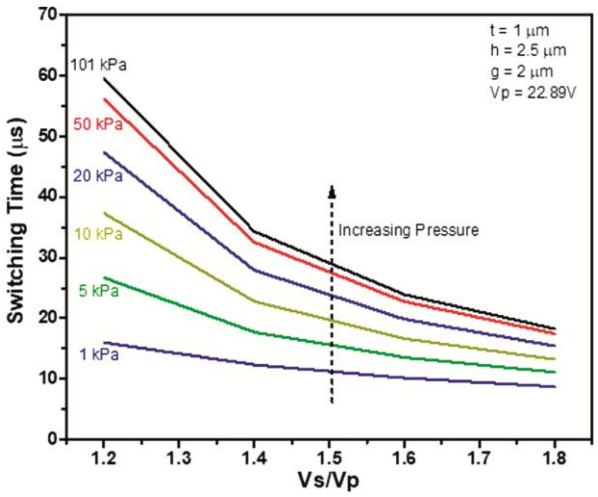

Fig. 8 — Switching time of micromirrorat different supply voltage.

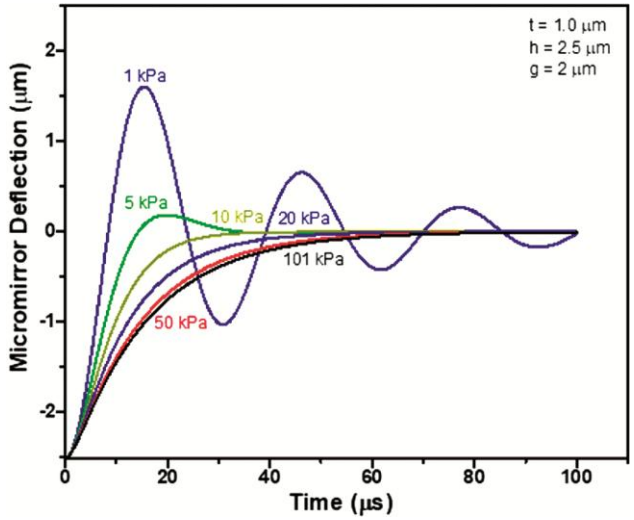

Fig. 9 — Release time of micromirror at different pressures.

The coefficient terms are calculated at different pressures, and the differential equations are solved with initial conditions of maximum displacement and zero velocity at the point of release given by

$$y(0) = -2.5\mu m \quad \ldots(15)$$

$$x(0) = 0 \quad \ldots(16)$$

The release response of the micromirror at different pressures is shown in Fig. 9.

The micromirror goes through an overshoot and multiple oscillations at pressures below 10 kPa before reaching a complete halt. At pressures above 10 kPa, the overshoot and oscillations are suppressed, and the micromirror attains a stable state much faster.The fluctuation in onboard supply voltage is accounted for

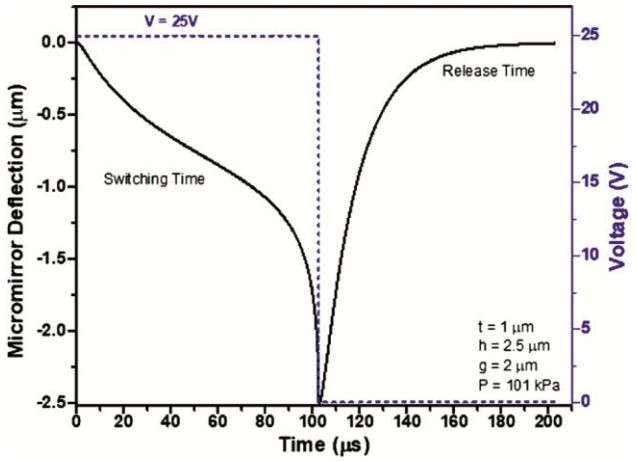

Fig. 10 — Complete switching cycle of micromirror at 101 kPa.

by driving the micromirror at 25 V, higher than the pull-in voltage but smaller than the maximum onboard supply of 28 V. The complete switching cycle of the micromirror at an actuation voltage of 25 V and 101 kPa pressure is shown in Fig. 10.

The micromirror takes 102 μs to achieve a tilted state and 95 μs to return to its initial position after removing the voltage. The accuracy of the analytical model is validated with the FEM results[4] and found to be in close agreement with a deviation of 8% only.

4 Conclusion

This paper presents an analytical approach to envisage a suitable operating pressure for driving an electrostatically actuated double-bridge micromirror for space-based multi-object spectroscopy applications. The electrostatic forces acting on the micromirror of size 200 μm × 200 μm are modeled using a parallel-plate capacitor approximation, and the squeezed-film damping effects, switching, and release time are investigated by solving the linearized Reynolds equation and equation of motion using the Runga-Kutta numerical iteration method in Matlab®. Under incompressible fluid approximation, the micromirror exhibits an overdamped response above 10 kPa pressure suitable for multiobject spectroscopy application. The results show that operating the micromirror at atmospheric pressure serves the triple purpose of dispensing away with the requirement of vacuum packaging and providing immunity from vibrations and oscillations without significantly affecting the switching speed. The micromirror exhibits a switching and release time of 102 μs and 95 μs, respectively at 25 V and 101 kPA. The analytical results are compared with the finite element

simulation results, and they agree within 8%. The simple analytical approach presented in this paper can be used to optimize the operating pressure and analyze the effect of squeezed-film damping on the transient response of different electrostatic MEMS structures.

Acknowledgment

The authors acknowledge the financial support from the Council of Scientific and Industrial Research, India.

References

1 Zamkotsian F, Lanzoni P, Noell W, et al. *Int Conf Space Opt—ICSO*, 10566 (2008) 5.
2 Zamkotsian F, Lanzoni P & Tangen K, Micromirror arrays for multi-object spectroscopy in space, In: Armandillo E, Cugny B, Karafolas N, Eds, *Int Conf Space Opt— ICSO 2010*, 10565 (2019) 514.
3 MacKenty J W & Stiavelli M A, *ASP Conf Ser*, 195 (2000) 443.
4 Kumar A, Kumar P, Bajpai A, Rangra K & Bansal D, *IEEE Trans Electron Dev*, 68 (2021) 5773.
5 Kumar A, Kumar P, Bajpai A, Rangra K & Bansal D, *IEEE Trans Electron Dev*, 67 (2020) 4392.
6 Reinhardt K C, Mayberry C S, Glaister D S, *J Spacecr Rockets*, 35 (1998) 837.
7 Shea H R, Reliability of MEMS for space applications. In: Tanner DM, Ramesham R, Eds, *European Space Agency, (Special Publication)*, 6111 (2006) 61110A.
8 Darling R B, Hivick C & Xu J, *Sens Actuators A Phys*, 70 (1998) 32.
9 Chen T H, Chiu J, Cheng C W, Lu M S C, *IEEE Sens J*, 19 (2019) 1653.
10 Najar F, Ghommem M & Abdelkefi A, *Int J Mech Sci*, 178 (2020) 105624.
11 Pan F, Kubby J, Peeters E, Tran A T & Mukherjee S, *J Micromech Microeng*, 8 (1998) 200.
12 Waldis S, Zamkotsian F, Clerc P A, Noell W, Zickar M & de Rooij N de, *IEEE J Sel Top Quantum Electron*, 13 (2007) 168.
13 Kim D H, Kim M W, Jeon J W, Lim K S & Yoon J B, *J Microelectromech Syst*, 18 (2009) 1382.
14 Rebeiz G M, *RF MEMS: Theory, Design, and Technology*, John Wiley & Sons, 2003.
15 Pandey A K, *Analytical, Numerical, and Experimental Studies of Fluid Damping in MEMS Devices*, Department of Mechanical Engineering, Indian Institute of Science, Bangalore, (2007).
16 Hosaka H, Itao K & Kuroda S, *Sens Actuators A Phys*, 49 (1995) 87.
17 Mo Y, Du L, Qu B, Peng B & Yang J, *Wirel Sens Netw*, 09 (2017) 178.
18 Andrews M K, Turner G C, Harris P D & Harris I M, *Sens Actuators A Phys*, 36 (1993) 219.
19 Seidel H, Riedel H, Kolbeck R, Mück G, Kupke W & Königer M, *Sens Actuators A Phys*, 21 (1990) 312.
20 Burgdorfer A, *J Basic Eng*, 81 (1959) 94.
21 Veijola T, Kuisma H, Lahdenperä J & Ryhänen T, *Sens Actuators A Phys*, 48 (1995) 239.
22 Younis M I, *MEMS Linear and Nonlinear Statics and Dynamics*. Springer US, (2011).
23 Chakraborty S, Chaudhuri A R & Bhattacharyya T K, *Int Conf Adv Comput, Control Telecommun Technol*, (2009) 184.